ENGINEERING RESEARCH JOURNAL (ERJ)

Vol. 1, No. 51 Jan 2022, pp.21-26

Journal Homepage: http://erj.bu.edu.eg

Impact Resistance of AISI 304L Stainless Steel Welded Joints at Low Temperatures

Eng. Abdullah Bader Aljeaan , Asst. Prof. Samah Samir Mohamed

Mechanical Engineering Department, Faculty of Engineering at Shoubra, Benha University, Cairo, Egypt

Abstract

In the present investigation, the impact energy of the AISI 304L austenitic stainless steel (ASS) alloy welded joints were evaluated at both ambient and low temperatures up to -80 °C. Moreover, regression analysis (RA) and artificial neural networks (ANN) techniques were used to develop models to predict the impact energy of the AISI 304L base alloy (BA) and the welded joints. A comparison between the two developed RA and ANN models was carried out. The results revealed that the impact energy of the AISI 304L base alloy and welded joints was found to be reduced with reducing the test temperature. However, the AISI 304L base alloy exhibited higher impact energy when compared with the welded joints. Such behavior was observed at both ambient and low temperatures. Both RA and ANN models can be used to predict the impact energy of the AISI 304L base alloy as well as the welded AISI 304L joints as a function of temperature at both ambient and low temperatures. The RA and ANN models exhibited mean absolute percentage error (MAPE) of 1.22% and 1.34% for the AISI 304L base alloy, respectively. While the RA and ANN models exhibited MAPE of 2.13% and 1.41% for the welded AISI 304L joints, respectively.

Keywords: AISI 304L, Impact Toughness, GTAW, Low Temperatures, Artificial Neural Networks.

1. Introduction

Stainless steels (SS) are the group of ferrous alloys that contain a minimum of approximately 11% chromium. They also- may include other elements like carbon (from 0.03% to greater than 1.00%), nitrogen, aluminum, silicon, sulfur, titanium, nickel, copper, selenium, niobium, and molybdenum [1,2]. Stainless steels are ideal materials for many applications where both the strength of steel and corrosion resistance are required. There are five main types of SS, which are primarily classified by their crystalline structure, typically, (1) austenitic SS, (2) ferritic SS, (3) martensitic SS, (4) duplex SS, and (5) precipitation hardening SS. The austenitic SS are the most weldable of the high-alloy steels and can be welded by all fusion and resistance welding processes.

The AISI 304 and AISI 304L SS are known also as 1.4301 and 1.307 SS, respectively. The AISI 304 SS is an austenitic grade. The AISI 304 SS is also known as 18/8 SS which is derived from the nominal composition of AISI 304 SS that contains 18% chromium and 8% nickel. The AISI 304 SS is used in heavy gauge components for improved weldability [3]. Type AISI 304L is the low carbon version of AISI 304. The carbon content of AISI 304L is limited to a maximum of 0.03%, which prevents sensitization (formation of chromium carbides along grain boundaries) during welding. The formation of chromium carbide reduces the corrosion resistance along the grain boundary. Therefore, the lower carbon content in AISI 304L minimizes the harmful carbide precipitation because of welding. In contrast, the

AISI 304L SS exhibits slightly lower mechanical properties than the AISI 304 SS [1].

In the present investigation, the impact resistance of the AISI 304L SS at both ambient and low temperatures were studied. Sheets made from AISI 304L were welded by gas tungsten arc welding (GTAW) technique using AISI 308L SS filler rod. The impact resistance of the 304L SS welded joints were evaluated at ambient, -20, -40, -60 and -80 ºC. The microstructure of the welded joints was also examined using optical metallurgical microscope (OMM). Regression analysis (RA) and artificial neural network (ANN) models were also developed to predict the impact energy with the temperatures for the welded joints.

2.EXPERIMENTAL PROCEDURES

The AISI 304L austenitic stainless steel (ASS) was adopted as a base alloy or base metal (BM). The chemical compositions of the AISI 304L ASS are listed in the Table (1).

Table (1). The chemical composition of AISI 304L austenitic stainless steel (wt.-%).

Base Alloy	Elements (wt.-%)							
	Cr	Ni	C	Mn	Si	P	S	Fe
AISI 304L	18.91	10.65	0.028	2.01	1.1	0.04	0.03	Bal.

The AISI 304L ASS was received in the form of large hot rolled plates with of thickness 10 mm. The AISI 304L ASS plates were cut into smaller plates having dimensions of 50 mm (width)× 600 mm (length)× 10 mm (thickness). The ER 308L filler material (filler rod) was used to weld the AISI 304L ASS [4].

The plates with the dimensions of 50 mm (width)× 600 mm (length) × 10 mm (thickness) were machined to get single V-groove with an angle of 60º as shown in Fig.1 (According to AWS D14.4/D14.4M:2019) [5]. Plates from AISI 304L ASS plates were welded using gas tungsten arc welding (GTAW) technique to form butt joints. The GTAW process was performed using (NEA, WSHE-315A, 2017, China) SMAW/GTAW welding machine. The GTAW process parameters used for welding the AISI 304L ASS plates are listed in Table 2.

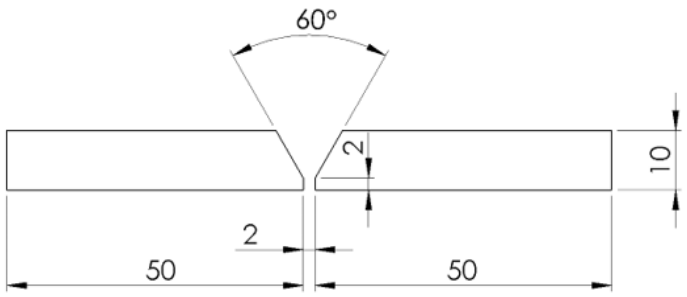

Fig 1. The joint configuration of AISI 304L ASS plates (dimensions in mm) according to AWS D14.4/D14.4M:2019.

Table 2. The GTAW process parameters used for welding AISI 304L ASS.

Process Parameter	Value
Constant Voltage (Volts)	40
Constant Ampere (Ampere)	220
Average Welding Speed (mm/sec)	10
Number of Passes	4

The micro structural examinations of the welded regions (WR) of the AISI 304L ASS were performed using KERN optical metallurgical microscope (OMM), Germany. The welded specimens were cut and ground under water using polishing/grinding machine. The specimens were ground using SiC emery papers with increasing grit number starts from 200 grit up to 1500 grit. After grinding, the welded specimens were exposed to polishing by using 0.1 μmAl_2O_3

(alumina) suspension. After polishing, the welded specimens were exposed to etching in an aqueous solution containing 33% HNO_3 and 33% HCl-acids for one minute. The etching procedures were performed according to ASTM E407-07 [6].

Charpy impact specimens having a V-notch were machined from the welded samples. The impact test specimens were prepared as per the ASTM E23 standard [7]. The impact specimens have 55 mm long and of square section with 10 mm sides, having at mid-length, a V-notch of 45° with a depth of 2 mm and a 0.25 mm radius of curve at the base of notch placed at the weld centerline. The specimen's V-notch was machined using an automatic notch machine.

Charpy impact tests were carried out for the AISI 304L SS base alloy (BA) as well as the welded joints at ambient and lower temperatures of -20, -40, -60 and -80 °C. The ethanol alcohol-based refrigeration chamber was used to cool the welded specimens to the desired temperatures. The specimens are first immersed in the ethanol to the desired temperatures. The temperature was measured by using a thermocouple immersed in the refrigeration chamber. After reaching the desired temperature, the specimen is immediately subjected to impact testing and the absorbed energy (in Joules) is recorded using a computerized system. The impact test was repeated three times and the average value of the impact energy is recorded. The JBW-500B, China, impact tester was used to perform the tests. The tester has a maximum energy of 300 joules with a 5.1 m/s hammer speed.

A regression analysis (RA) was performed to correlate the impact energy of the BA and AW AISI 304L ASS with the temperature. The linear RA was used to correlate the input factor (i.e., temperature) with the output factor (i.e., absorbed energy).The artificial neural network (ANN) technique was also used for modeling the influence of temperature on the impact energy of welded and unwelded samples. The ANN model was based on Multi-Layer Perceptron (MLP) neural networks.

The mean absolute percentage error (MAPE) was calculated to define the accuracy of the generated regression or ANN models. The MAPE can be calculated by using the following equation [8]:

$$\mathrm{MAPE} = \frac{100\%}{n} \sum_{t=1}^{n} \left| \frac{A_t - F_t}{A_t} \right| \quad \ldots(1)$$

where A_t is the actual (experimental) value and F_t is the predicted value. The absolute value in this ratio is summed for every predicted point in time and divided by the number of fitted points *n*.

3. RESULTS AND DISCUSSION

3.1. Microstructural Examinations

A typical microstructure of AISI 304L ASS welded zone (WZ) is shown in Fig. 2 The welded region consists of the weld metal (WM) as well as the heat-affected zone (HAZ). The HAZ defined as a part of BM that is close to WM region. The HAZ is affected by the heat of welding. The base material (BM) region is also shown in the micrograph. Figure 3 shows higher magnification of the WM as well as BM regions in the WZ. The microstructure of the WM region (Fig. 3b) reveals dendritic structure with predominantly fine diffusion of carbides. The carbides precipitate because the alloy rich austenite can no longer accommodate all the W and Mo left by the preexisting ferrite. This is also because of the reaction that both base metal (304L) and filler metal (ER308L) are of extra low carbon version with controlled welding parameter [9].

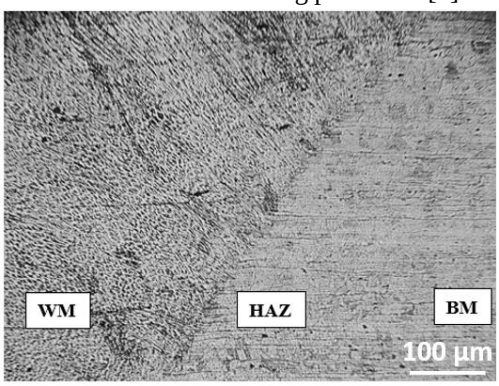

Fig 2. Microstructure of the welded region.

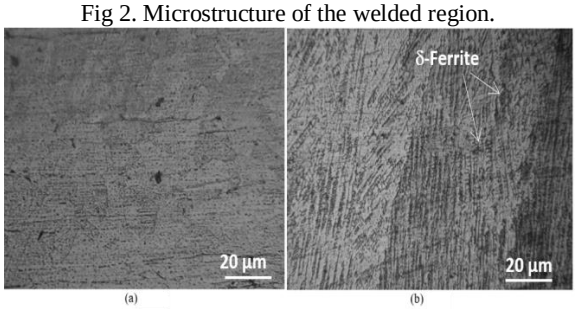

Fig 3. Higher magnification micrographs for the microstructure of (a) AISI 304L base alloy and (b) the weld metal (WM) region.

The microstructure of the BM region consists mainly of γ-austenite equiaxed grains with small amount of δ-ferrite in grain boundaries. Under equilibrium conditions of solidification, the microstructure of the AISI 304L ASS consists mainly of (γ) austenite. However, during the non-equilibrium conditions or rapid solidification, the high cooling rate resulted in incomplete δ/γ transformation, and some metastable δ-ferrite unavoidably remained [10-13]. Therefore, after solidification more δ-ferrite was retained in the weld metal.

3.2. Impact Resistance

Figure 4 shows the variation of the impact energy with the temperature for both welded and unwelded AISI 304L ASS samples. The results revealed that the impact energy is reduced with reducing the temperature. This was noticed for both the welded and unwelded specimens. The ambient temperature showed the highest impact energy, while at -80 °C, the lowest impact energy was observed. Moreover, the unwelded specimens exhibited higher impact energies when compared with the welded ones at the same test temperature. For example, at test temperature of -20 °C, the unwelded and welded AISI 304L ASS exhibited average impact energies of 196 J and 173 J, respectively.

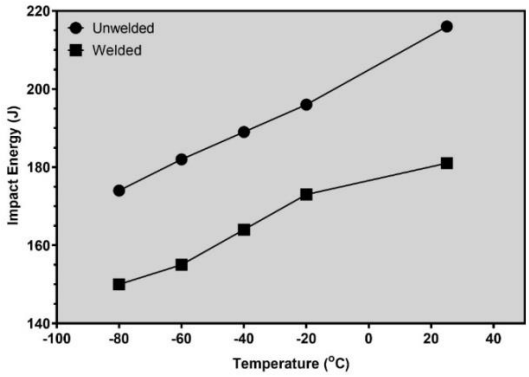

Fig 4. The variation of the impact energy with the temperature for both welded and unwelded AISI 304L ASS samples.

3.3. Regression Modelling

Equation 2 shows the correlation between the absorbed impact energy in Joules with the test temperature for the AISI 304L unwelded or base alloy (BA) samples.

$$IE_{BA} = 205 + 0.396\ T \quad \ldots (2)$$

Where IE_{BA} is the impact energy of the base alloy in Joules and the T is the test temperature in Celsius. The developed equation has R^2 and MAPE values of 0.959 and 1.22%, respectively. Figure 5 shows a comparison between the predicted and the experimental impact energies obtained at several temperatures. It is clear that both (i.e. the predicted and the experimental) energies are close to each other.

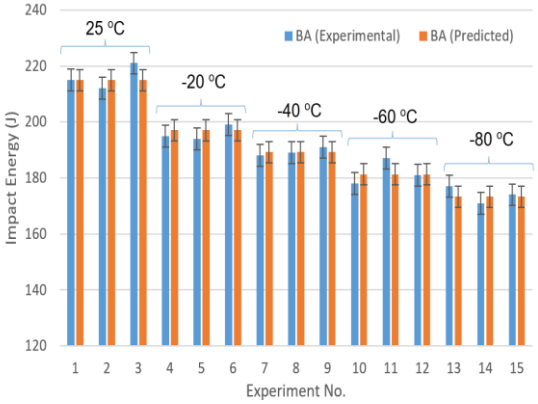

Fig 5. Comparison between the predicted and the experimental impact energies for the unwelded AISI 304L base alloy (BA) at several temperatures.

Equation 3 shows the correlation between the absorbed impact energy with the test temperature for the welded AISI 304L ASS samples.

$$IE_W = 175 + 0.303\ T \quad \ldots (3)$$

Where IE_W is the impact energy of the welded AISI 304L ASS in Joules and the T is the test temperature in Celsius. The developed equation has R^2 and MAPE values of 0.918 and 2.13%, respectively. Figure 6 shows a comparison between the predicted and the experimental impact energies obtained at several temperatures for the welded AISI 304L ASS samples. Again, the predicted and the experimental energies are close to each other.

According to the above results, it can be concluded the developed regression model for the unwelded samples has higher accuracy when compared with the regression model for welded samples. This may explain by the more complex microstructure obtained after welding in the welded metal region of the AISI 304L ASS. However, both models have high accuracy and can be used to predict the impact energy of both

welded and unwelded AISI 304L samples at different temperatures.

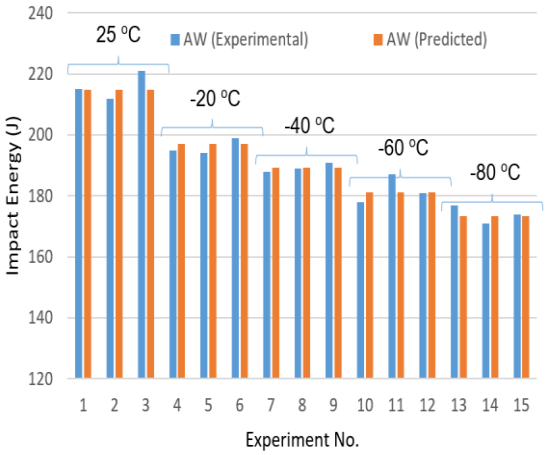

Fig. 6. Comparison between the predicted and the experimental impact energies for the welded AISI 304L ASS samples at several temperatures.

3.4. Artificial Neural Networks Modelling

The developed ANN MLP models for the AISI 304L ASS unwelded or base alloy (BA) and the welded joints have MLP 1-3-1 and MLP 1-7-4 structures, respectively. The ANN model structure consists of three layers, typically, the input layer, the hidden layer, and the output layer. The input layer has one input parameter, namely, the test temperature (T). The hidden layer has three (unwelded) or seven (welded) elements. The hidden layers for the unwelded and welded joints models have logistic and Tanh activation function, respectively. The output layer has one factor, namely, the impact energy. The developed ANN MLP models showed training performance of 97.97% and 96.77%, for the unwelded and welded joints, respectively.

Figures 7 and 8 illustrate comparison between the experimental and predicted impact energies obtained from ANN. The perfect prediction is when all the plotted points were on the 45° line. The accuracy of the ANN model could be evaluated by the closeness of the plotted points to the 45° line.

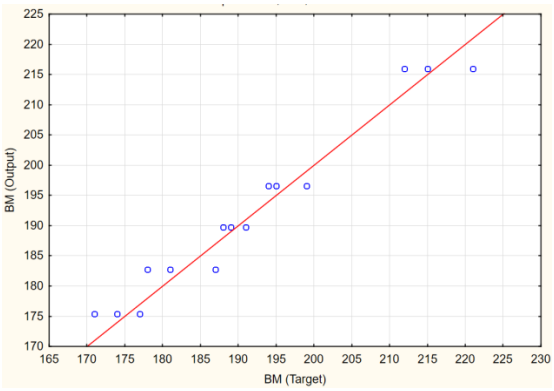

Fig. 7. Comparison between the ANN predicted and the experimental impact energies for the unwelded AISI 304L ASS base alloy (BA) at several temperatures.

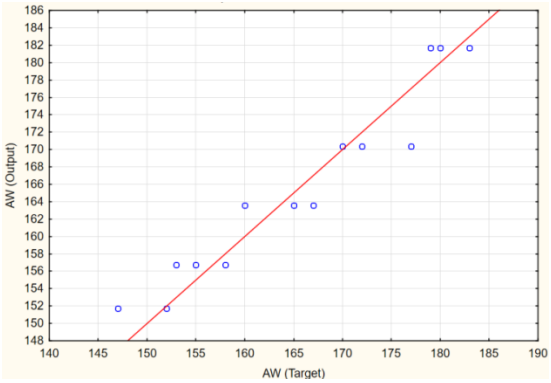

Fig 8. Comparison between the ANN predicted and the experimental impact energies for the welded AISI 304L ASS alloy at several temperatures.

The developed ANN models for unwelded and welded joints showed MAPE of about 1.34% and 1.4%, respectively. For the AISI 304L ASS base alloy, the RA model has slightly higher accuracy when compared with the ANN model. In contrast, for the AISI 304L ASS welded joints, the ANN model showed better accuracy when compared with the RA model.

4. CONCLUSIONS

Based on the results obtained from the present investigation, the following conclusions of significance are drawn: -

1. The impact energy of the AISI 304L base alloy and welded joints was found to be reduced with reducing the test temperature. The ambient temperature showed the highest impact energy, while at -80 °C, the lowest impact energy was observed. Moreover, the AISI 304L base alloy (unwelded) specimens exhibited higher impact energy when

compared with the welded ones at the same test temperature.

2. For the AISI 304L base alloy, the regression analysis (RA) model showed slightly better accuracy when compared with the artificial neural networks (ANN) model. In contrast, for the AISI 304L welded joints, the ANN model showed slightly better accuracy when compared with the RA model.
3. Both RA and ANN models can be used to predict the impact energy of the AISI 304L base alloy as well as the welded AISI 304L joints as function of the temperature at both ambient and low temperatures.
4. The RA and ANN models exhibited mean absolute percentage error (MAPE) of 1.22% and 1.34% for the AISI 304L base alloy, respectively. While the RA and ANN models exhibited MAPE of 2.13% and 1.41% for the welded AISI 304L joints, respectively.

REFERENCES

[1] ASM Handbook, "Introduction to Stainless Steels", ASM International, 2000.

[2] Aalco Metals Ltd., "Introduction to Stainless Steels", pp. 1-5.

[3] J.A. Brooks, J.C. Lippold, "Selection of Wrought Austenitic Stainless Steels", In ASM Handbook, Vol 6, Welding, Brazing and Soldering, 1993.

[4] ESAB, "Welding Filler Metal Databook", USA, 2016.

[5] American Welding Society Standards, AWS D14.4/D14.4M, "Specification for the Design of Welded Joints in Machinery and Equipment", 2019.

[6] ASTM E407 – 07, "Standard Practice for Microetching Metals and Alloys", 2015.

[7] ASTM E23-18, "Standard Test Methods for Notched Bar Impact Testing of Metallic Materials", 2018.

[8] B. S. Everitt; A. Skrondal, "The Cambridge Dictionary of Statistics", Cambridge University Press, 2010.

[9] G. Britto Joseph, G. Mageshwaran, R. Ajith Kumar, R. B. Durai Raj, JeyaJeevahan, Mani Kunjan, "Characteristics Studies of Stainless Steel (AISI Type 304L) Welded by ER310L Filler Using TIG Welding", Int. J. Chem. Sci., 14(4), 2016, pp. 2527-2534.

[10] E. Ahmadi, A. R. Ebrahimi, R. Azari Khosroshahi, "Welding of 304L Stainless Steel with Activated Tungsten Inert Gas Process (A-TIG)", International Journal of ISSI, 10(1), 2013, pp. 27-33.

[11] K. Prasad Rao, A. Uma Maheshwar Rao, G. J. Gururaja, "Effect of delta ferrite content on the corrosion resistance of type 316 clad metals", Materials and Corrosion, 39, 1988, pp. 135-142.

[12] J. C. Lippold, D. J. Kotecki, "Welding metallurgy and weldability of stainless steels", Wiley Interscience; 1Ed., ISBN 9780471473794, 2005.

[13] V. Shankar, T. P. Gill, S. L. Mannan, "Solidification cracking in austenitic stainless-steel welds", Sadhana, 28, 2003, pp. 359-382.